Electronic Supplementary Material

Cuprous Sulfide Intermediate Assisted Synthesis of $PtCu_3$ Intermetallic Electrocatalysts in Multigramm Scale for Oxygen Reduction

Shi-Long Xu[a,b], Peng Yin[a,b], Lu-Jie Zuo[b], Shi-Yi Yin[b], Ming Zuo[b], Wanqun Zhang[b], Xian-Zhu Fu[a]*, Hai-Wei Liang[b]*

[a] College of Materials Science and Engineering, Shenzhen University, Shenzhen, 518060, China.

[b]Hefei National Laboratory for Physical Sciences at the Microscale, Department of Chemistry, University of Science and Technology of China, Hefei, 230026, China.

E-mail: xz.fu@szu.edu.cn (X.-Z. F.)；hwliang@ustc.edu.cn (H.-W. L.)

Table of Contents

S1. Methods and syntheses of materials

Materials. All chemicals were from commercial sources and were used without further purification. The chemicals were purchased from Sinopharm Chemical Reagent Co. Ltd., China, including hexachloroplatinic hexahydrate ($H_2PtCl_6 \cdot 6H_2O$, 99%), copper chloride hexahydrate ($CuCl_2 \cdot 6H_2O$, 99%), and sulfuric acid (H_2SO_4, 95%~98%). 2,2'-bithiophene (98%) was purchased from J&K Scientific Ltd. Perchloric acid ($HClO_4$,70−72%) was purchased from Sigma-Aldrich. Deionized (DI) water (18.2 MΩ/cm) used in all experiments was prepared by passing through an ultra-pure purification system.

Synthesis of S-BP support and $PtCu_3$ catalysts. The S-doped Black Pearls 2000 (denoted as S-BP) were prepared by the modified cobalt-assisted carbonization of molecular precursors with BP as support, according to the previously reported method.[1, 2] In a typical synthesis, 25 g of 2,2'-bithiophene, 25 g of BP support and 12.5 g of $Co(NO_3)_2 \cdot 6H_2O$ were first dispersed in tetrahydrofuran solution. The solvent was then removed by oil bath dry under 80 °C with stirred continuously. The obtained dried powder was subsequently carbonized under flowing N_2 for 2 hours at 800 °C. Finally, the carbonized product was successively treated by 2 M H_2SO_4 leaching for three times to remove cobalt species and yield the S-BP supports.

The $PtCu_3$/S-BP catalysts were prepared via a conventional impregnation process of aqueous solution containing H_2PtCl_6, $CuCl_2$ and S-BP support. In general, H_2PtCl_6 and $CuCl_2$ were mixed with 100 mg S-BP support in a 100 mL round bottom flask containing 50 mL DI water. The total metal content was controlled to be 20 wt% with Cu/Pt =3.5, (the Pt content was around 10 wt%). After stirring overnight, the mixture was subjected to ultrasonic treatment for 1 h before drying by using a rotary evaporator. Finally, the dried powder was then subjected to high-temperature H_2-reduction treatment in flowing 5 % H_2/Ar at 300-1100 °C for 2 hours before naturally cooling down to room temperature. For comparison, the $PtCu_3$/BP catalyst was synthesized by a similar process with undoped BP as the support. The Pt contents in the final $PtCu_3$ catalysts were quantified by the inductively coupled plasma atomic emission spectrometry (ICP-AES) measurements (Table S1).

Electrochemical measurements. For RDE test, the optimal catalysts are $PtCu_3$/S-BP-1100 and $PtCu_3$/BP-800. The reduction temperatures are 1100 and 800 °C corresponding to $PtCu_3$/S-BP and $PtCu_3$/BP, respectively. Prior to the electrochemical test, all $PtCu_3$ catalysts were treated with mild air oxidation at 210 °C for 2 h before electrochemical measurements to fully expose the surface. The catalyst ink was prepared by dispersing 5 mg of electrocatalysts in 2.5 mL of isopropanol through ultrasonication, followed by addition of 30 mL of Nafion ionomer (Sigma-Aldrich, 5 wt %). To prepare a uniform thin-film electrode, the catalyst ink was pipetted and drop casted on the glassy carbon substrate. Catalyst loadings were set to 20.4 μg_{Pt} cm^{-2} for $PtCu_3$/S-BP, $PtCu_3$/BP catalyst and Pt/C (Johnson Matthey Co., 20 wt %).

Electrochemical measurement was performed with a three-electrode electrochemical cell using CHI 760E electrochemical workstation (Shanghai Chenhua, China). A rotating disk glassy-carbon with diameter of 5 mm (Pine Instruments) was used as working electrode. Hg/Hg_2SO_4 and Pt foil was used as the reference electrode and counter electrode. All potentials in this work are with respect to the reversible hydrogen electrode (RHE). The Hg/Hg_2SO_4 reference electrode was calibrated in pure H_2-saturated 0.1 M $HClO_4$. Before measurements, the catalysts were scanning from +0.05 to +1.05 V (vs. RHE) until a stable cyclic voltammetry (CV) curve was collected. Linear sweep voltammetry (LSV) was then measured from +0.05 to +1.05 V (vs. RHE) in O_2-saturated 0.1 M $HClO_4$ with scan rate of 10 mV s^{-1}. The capacitance current was obtained with the same LSV test in N_2-saturated 0.1

M $HClO_4$. The rotating speed of working electrode was controlled at 1600 r.p.m. in the LSV tests. The electrochemically active surface area (ECSA) was tested with the CO stripping, which was carried by first bubbling high-purity CO into 0.1 M $HClO_4$ electrolyte and retaining potential at +0.05 V (vs. RHE) for 10 min, followed by bubbling pure N_2 into the electrolyte for 5 min. Then the voltammetry curve was collected by scanning from +0.05 to +1.05 V (vs. RHE) with a scanning rate of 50 mV s^{-1}. The accelerated degradation test (ADT) was scanned from 0.6 to 0.95 V in N_2-saturated solution of 0.1 M $HClO_4$. The Koutecky−Levich (*K*−*L*) plots were obtained at various rotating speeds. The electron transfers number (*n*) can be calculated from the K−L equation:

$$\frac{1}{j} = \frac{1}{j_L} + \frac{1}{j_K} = \frac{1}{Bw^{1/2}} + \frac{1}{j_K}$$

$$B = 0.62nAFC_oD^{2/3}V^{-1/6}$$

where *j* is the apparent current density, j_K and j_L are the kinetic and limiting current densities, *w* is the angular velocity of the disk, *n* is the electron transfer number, *A* is the area of the electrode (0*:*196 cm^2), *F* is the Faraday constant (96485 C mol^{-1}), C_0 is the bulk concentration of O_2 (1.26×10^{-6} mol cm^{-3}), D_0 is the diffusion coefficient of O_2 in electrolytes (1.93×10^{-5} cm^2 s^{-1}), and *V* is the kinematic viscosity of the 0.1 M $HClO_4$ (1.01×10^{-2} cm^2 s^{-1}).[3]

Hydrogen peroxide yields and the electron transfer number (*n*) can be calculated through the following equations:

$$H_2O_2\ yield\ (\%) = 200 \times \frac{\frac{I_r}{N}}{I_d + \frac{I_r}{N}}$$

$$n = 4 \times \frac{I_d}{I_d + \frac{I_r}{N}}$$

where I_d and I_r are the disk and ring currents, respectively. The current collection efficiency for the Pt ring is $N = 0.37$. The ring potential is kept at a potential of 1.2 V/RHE.

Characterizations. High-angle annular dark-field (HAADF) images were collected on FEI Talos F200X operated at 200 kV. Energy-dispersive x-ray spectroscopy (EDS) mappings and line scans were obtained on FEI Talos F200X, equipped with a Super XEDS system (four systematically arranged windowless silicon drift detectors) at 200 kV. N_2 adsorption was carried with a Quantachrome ASiQ gas sorption analyzer, and the data were collected at liquid nitrogen temperature (77 K). Temperature-programmed reduction (TPR) of all catalysts were performed by using a Quantachrome ASiQ gas sorption analyzer equipped with TCD to measure the consumption of hydrogen. The temperature was set at a ramp rate of 10 °C min^{-1}, and the reducing gas of 10 vol% H_2 balanced Ar was set at a flow rate of 50 ml min^{-1}. The pore size distribution (PSD) plot was recorded from the adsorption branch of the isotherm based on the quenched solid density functional theory (QSDFT) model. Powder X-ray diffraction (PXRD) patterns were obtained on a Philips X'pert Pro Super diffractometer with a Cu Kα line (λ = 1.5418 Å) radiation source, with the operation voltage and operation current being 40 kV and 50 mA, respectively. The content of metal elements in the catalysts was measured by ICP-OES (Optiman 7300 DV, PerkinElmer). X-ray photoelectron spectroscopy (XPS) measurements were carried out on an ESCALAB MKII instrument equipped with an Mg Kα source (hν = 1253.6 eV), operating at 150 W and a spot size of 400 mm. For the narrow scans, an analyzer pass energy of 30 eV was applied. The X-ray absorption

spectroscopy (XAS) spectra at the Pt L-edge and Cu K-edge were obtained on the 1W1B beamline of Beijing Synchrotron Radiation Facility (BSRF) operated at 2.5 GeV and 250 Ma.

S2. Supporting figures

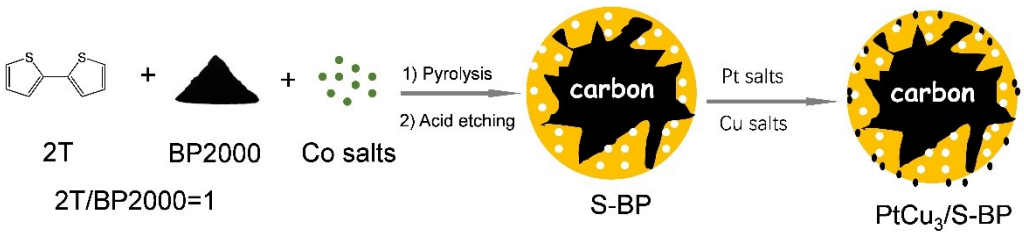

Fig. S1. Schematic illustration of the formation process for S-BP support and $PtCu_3$/S-BP.

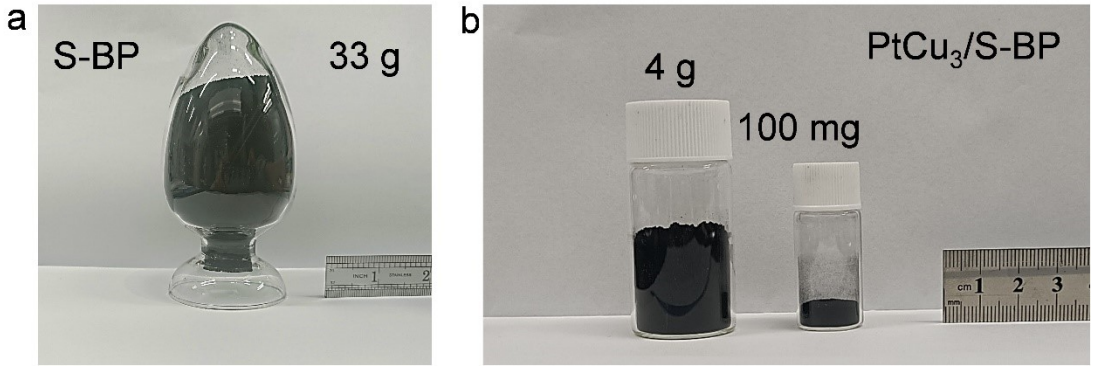

Fig. S2. (a-b) The picture of gram-scale S-BP support (a) and $PtCu_3$/S-BP catalyst (b).

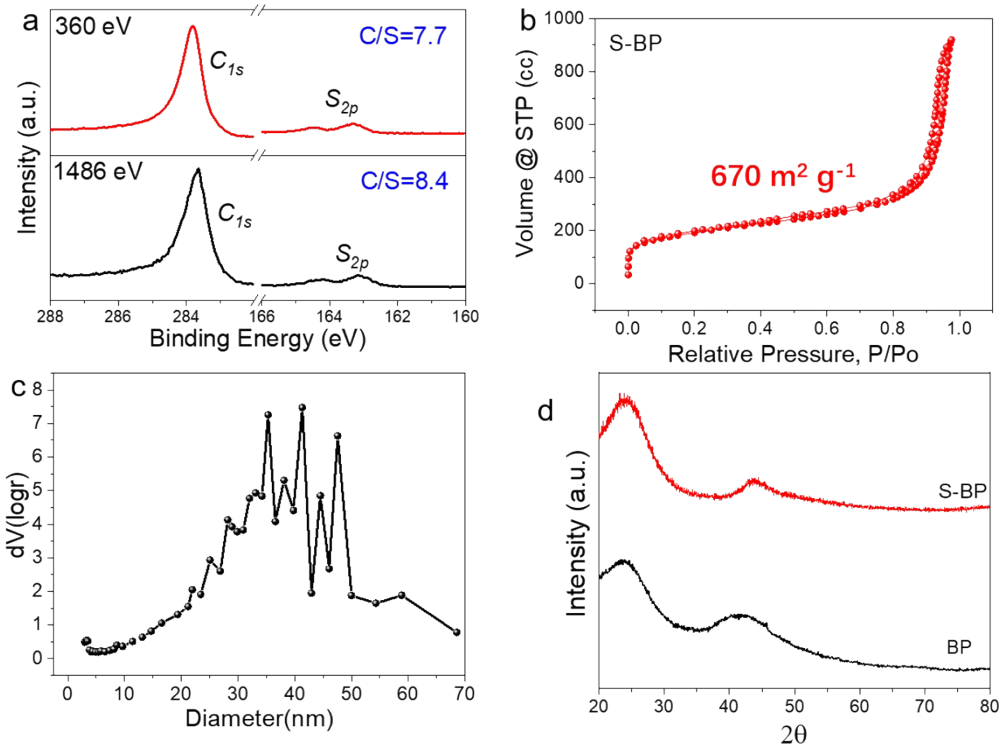

Fig. S3. Characterization of the S-BP support. (a) Synchoron radiation photoelectron spectroscopy and (b) Nitrogen sorption isotherms, (c) pore size distributions and (d) PXRD pattern of S-BP and BP support. No apparently XRD pattern change was observed after S doping.

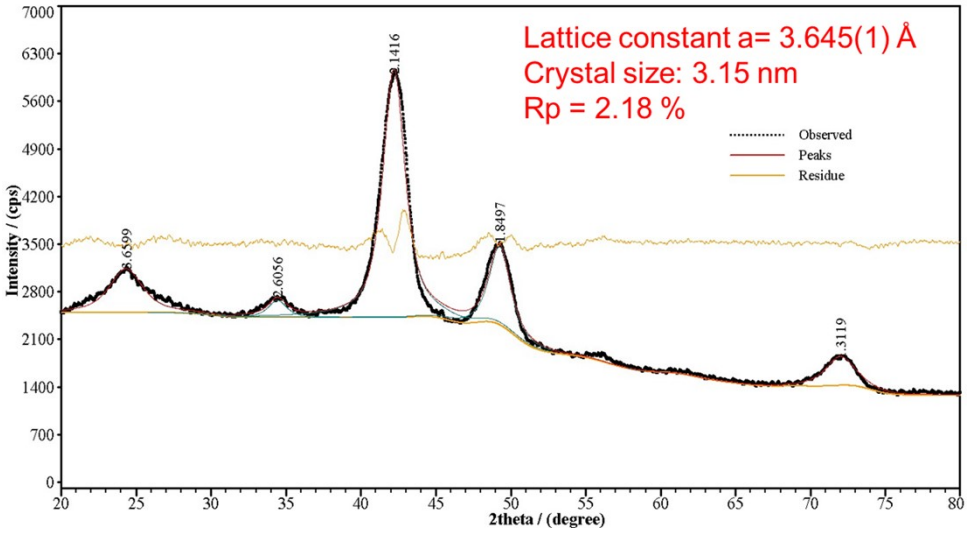

Fig. S4. XRD and Rietveld refinement patterns for $PtCu_3$/S-BP. The tested XRD patterns are shown as black circles. The difference and the background profiles are shown as yellow and green curves, respectively.

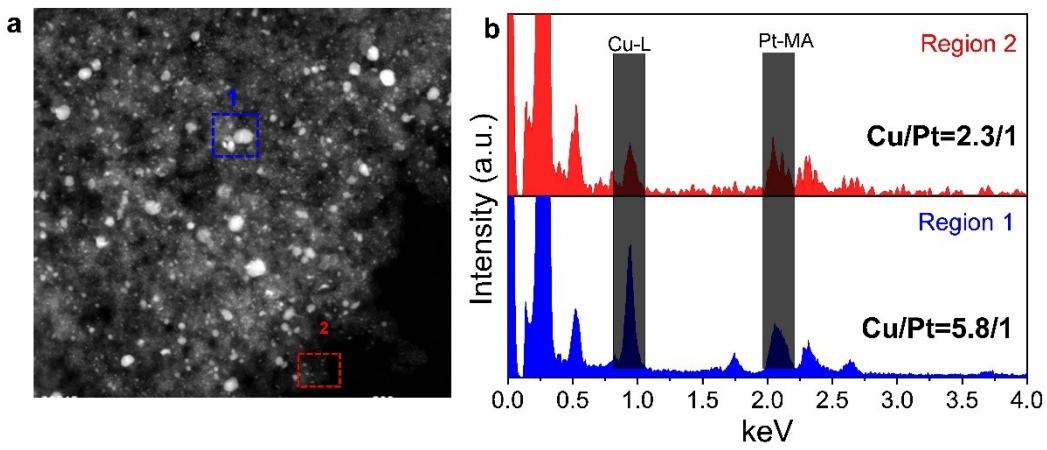

Fig. S5. (a) HAADF images and (b) EDS analysis of read region and blue region in a, showing that large particles were Cu-rich $PtCu_3$ IMC and small particles were PtCu alloy with a stoichiometric Cu/Pt ratio < 3.

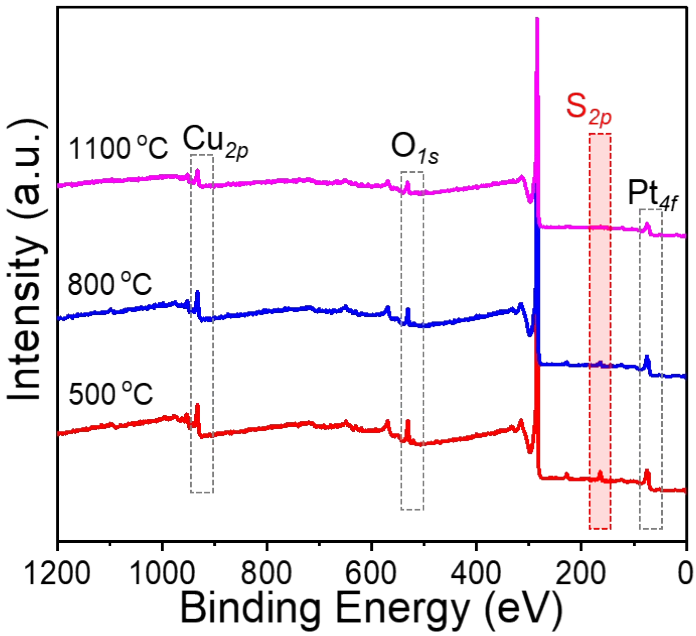

Fig. S6. XPS survey spectra of the $PtCu_3$/S-BP catalyst at different temperatures (500 °C,800 °C,1100 °C).

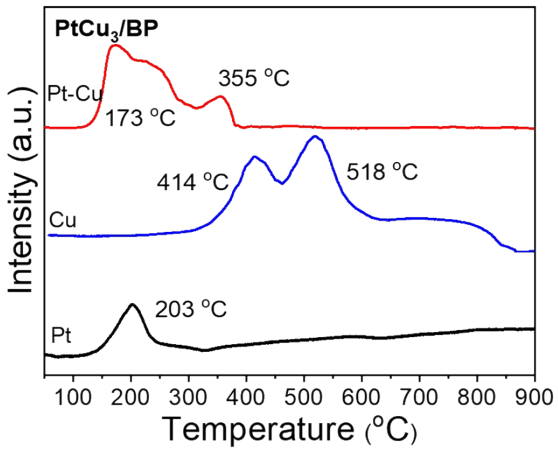

Fig. S7. H_2-TPR profiles of $PtCu_3$/BP samples. Although Cu complexes are very difficult to reduce over BP carbon support and require temperatures of 518°C, alloying Pt-Cu enabled us to observe hydrogen spillover–assisted reduction of Cu cations by Pt at a temperature of 355°C. No reduction peaks were observed over 400 °C for the Pt-Cu/BP sample, which confirmed the complete reduction of Pt/Cu species.

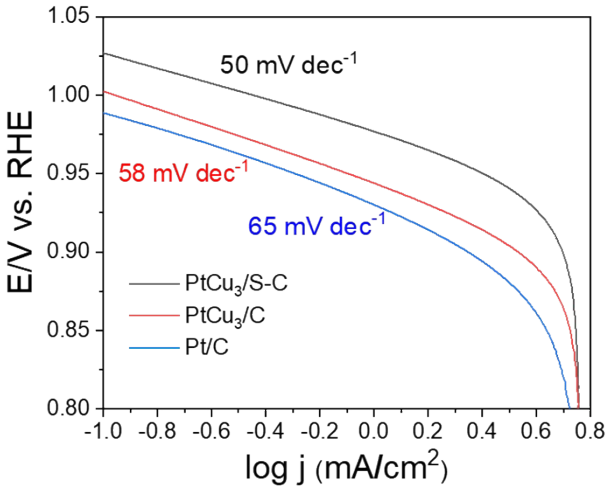

Fig. S8. Tafel curves of $PtCu_3$/S-BP, $PtCu_3$/BP and commercial Pt/C catalyst in 0.1 M $HClO_4$ solution.

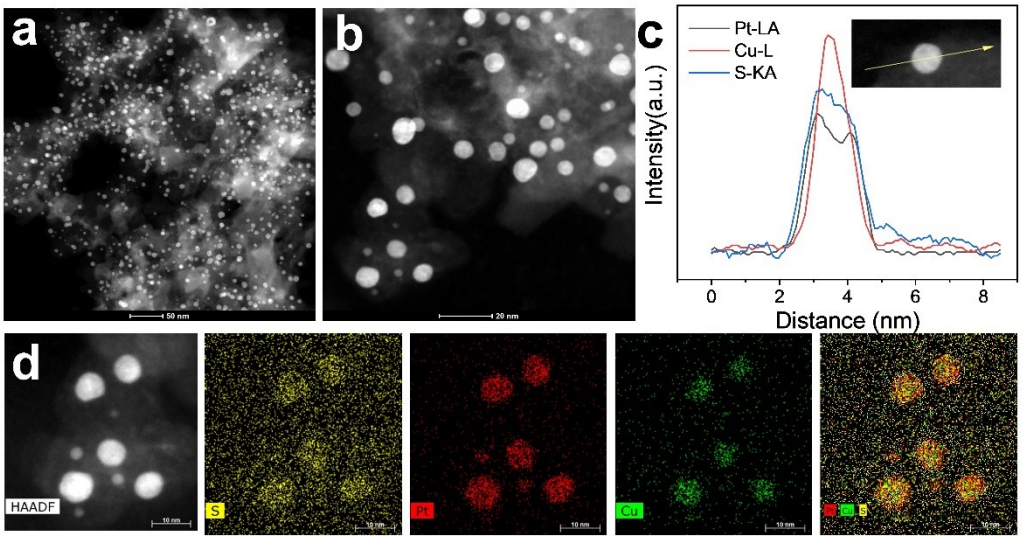

Fig. S9. (a-b) HAADF, (c) EDS-line scan and (d) EDS-mapping of $PtCu_3$/S-BP-1100 catalysts of electrochemistry test, showing $PtCu_3$@Pt core-shell structure.

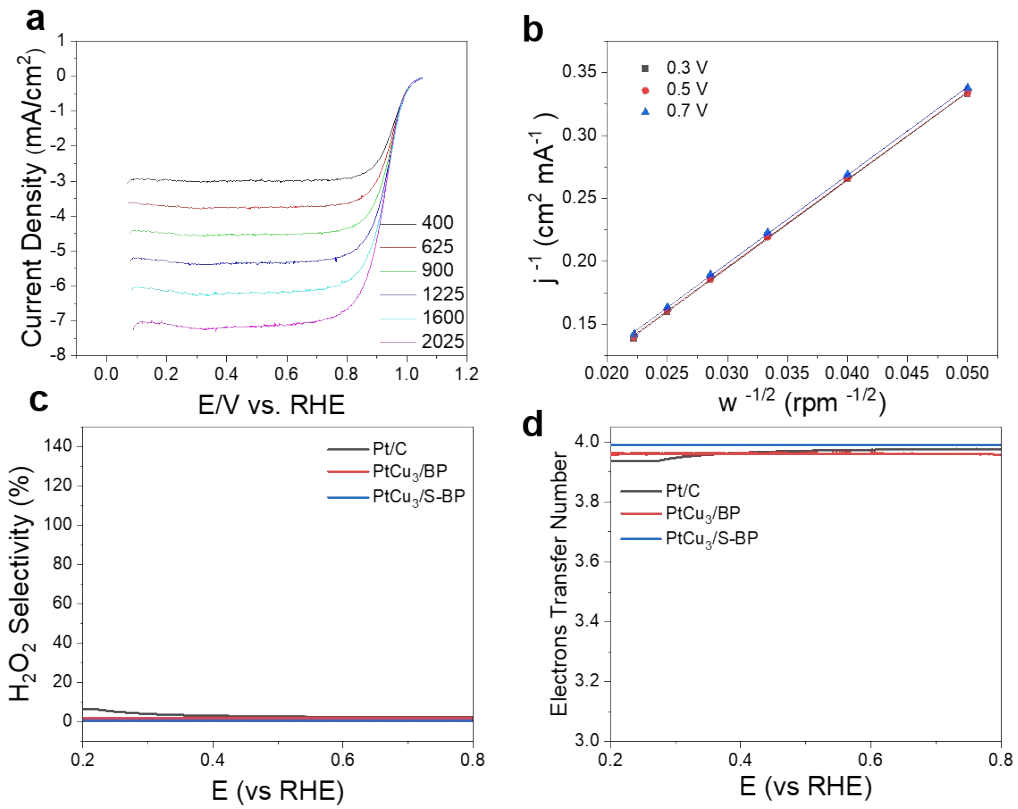

Fig. S10. (a-b) ORR polarization curve (a) and K−L plots (b) at different potentials for the $PtCu_3$/S-BP catalyst at various revolutions per minute (rpm). (c-d) Calculated selectivity (c) and electron transfer number (d) of the samples towards H_2O_2 at various potentials.

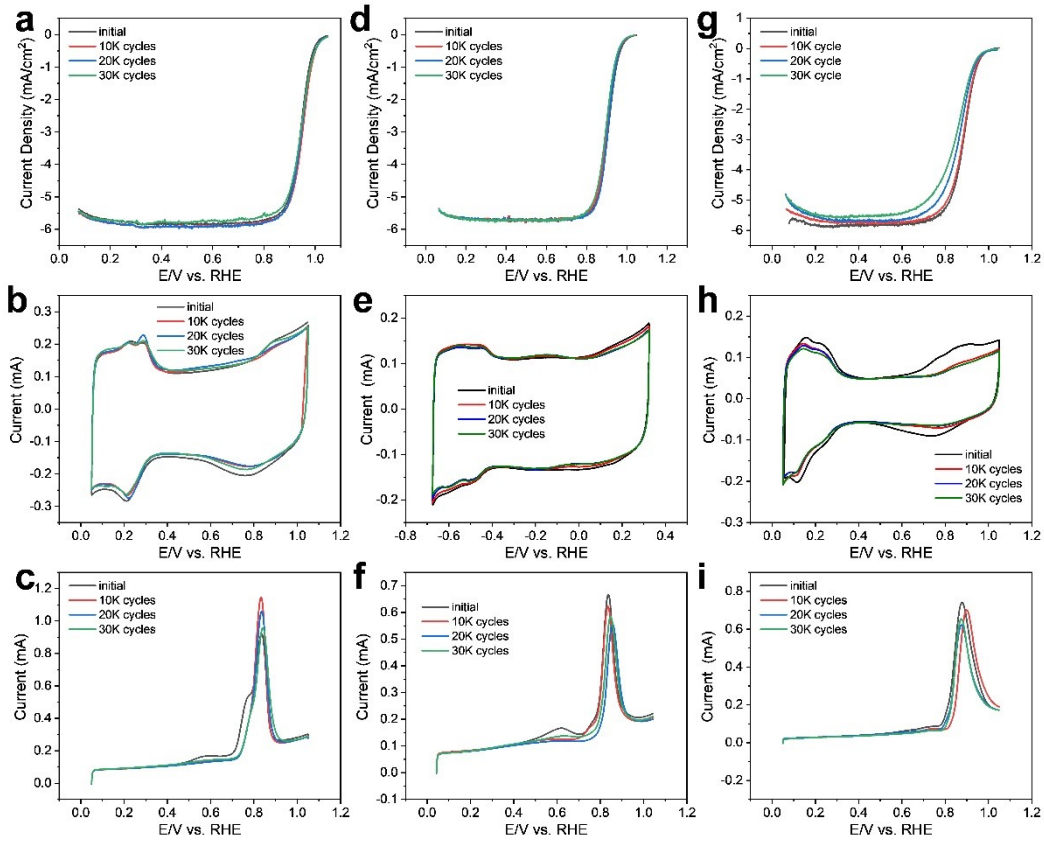

Fig. S11. RDE LSV, CV, and CO stripping curves of (a-c) $PtCu_3$/S-BP, (d-f) $PtCu_3$/BP and (g-i) commercial Pt/C catalyst after ADT tests.

S3. Supporting tables

Table S1. ICP analysis results of the $PtCu_3$ IMC catalyst.

Samples	Cu (wt%)	Pt (wt%)	Cu/Pt
$PtCu_3$/S-BP-1100	7.10	8.76	3.14
$PtCu_3$/BP-800	10.4	9.7	3.22

Table S2. XPS analysis results of the S-BP support.

Samples	C (wt%)	S (wt%)	N (wt%)	O (wt%)	Co (wt%)	C/S
S-BP	86.0	8.6	0.9	3.9	0.6	26.6

Table S3. XPS analysis results of the $PtCu_3$/S-BP catalyst.

Samples	C (wt%)	S (wt%)	Pt (wt%)	O (wt%)	Cu (wt%)
$PtCu_3$/S-BP-500	79.89	4.4	5.74	3.43	6.54
$PtCu_3$/S-BP-800	83.19	2.62	5.07	2.77	6.34
$PtCu_3$/S-BP-1100	89.92	0.83	3.67	1.73	3.84

Table S4. Summary of ORR performance of the Pt-Cu alloy catalysts.

	Sample	MA ($A\ mg_{Pt}^{-1}$)	SA ($mA\ cm_{Pt}^{-2}$)	Reference
1	$PtCu_3$/S-BP	3.16	4.42	Our work
2	O-PtCuNF/C	2.47	4.69	4
3	$PtCu_3$/C-CO	2.41	2.62	5
4	PtCu-600	1.92	1.37	6
5	Int-PtCuN/KB	1.15	1.18	7
6	PdCu B_2@Pt-Cu/C	2.55	4.33	8
7	$PtCu_3$/C	2.57	2.82	9
8	$PtCu_3$/S-C	4.2	3.8	1
9	PtCu nanoframes	0.82	1.24	10
10	PtCu nanotubes	0.1	0.23	11
11	hollow PtCu NPs	0.42	1.28	12
12	dealloyed $PtCu_3$ NPs	0.41	0.87	13
13	PtCu alloy octahedral nanoframes	0.28	0.5	14
14	$PtCu_3$@PWOx/C	3.94	3.3	15
15	$PtCu_3$/rGO	0.68	0.65	16
16	Dealloyed Core-Shell Pt-Cu	0.54	/	17
17	PtCuCo@Co-N-C	1.14	/	18
18	Pt-Cu-Co NPs	0.48	/	19
19	Pt-Cu-Mn NPs	0.466	1.27	20
20	PtCoNiCu/rGO	0.79	/	16
21	$Pt_2CuW_{0.25}$ Ternary alloy	0.75	1.43	21

Table S5. Summary of ORR performance of the $PtCu_3$/S-BP, $PtCu_3$/BP and commercial Pt/C catalysts before and after ADT tests.

Catalysts	CO-stripping ($m^2\ g_{Pt}^{-1}$)	MA ($A\ mg_{Pt}^{-1}$)	SA ($mA\ cm_{Pt}^{-2}$)
$PtCu_3$/S-BP	71.58	3.16	4.42
10 K	73.03	2.79	3.81
20 K	72.39	2.55	3.52
30 K	70.42	2.28	3.24
$PtCu_3$/BP	39.44	0.62	1.57
10 K	37.43	0.60	1.60
20 K	35.67	0.52	1.44
30 K	33.2	0.40	1.22
Commercial Pt/C	74.18	0.28	0.38
10 K	64.7	0.26	0.41
20 K	56.1	0.15	0.27
30 K	49.9	0.12	0.24

S4. References

1. Yang, C.-L.; Wang, L.-N.; Yin, P.; Liu, J.; Chen, M.-X.; Yan, Q.-Q.; Wang, Z.-S.; Xu, S.-L.; Chu, S.-Q.; Cui, C.; Huanxin, J.; ZhuJunfa; Yue, L.; Jianglan, S.; Hai-Wei, L., Sulfur-anchoring synthesis of platinum intermetallic nanoparticle catalysts for fuel cells. *Science* **2021,** *374* (6566), 459-464.

2. Wu, Z.-Y.; Xu, S.-L.; Yan, Q.-Q.; Chen, Z.-Q.; Ding, Y.-W.; Li, C.; Liang, H.-W.; Yu, S.-H., Transition metal–assisted carbonization of small organic molecules toward functional carbon materials. *Sci. Adv.* **2018,** *4* (7), eaat0788.

3. Wang, D.; Xin, H. L.; Hovden, R.; Wang, H.; Yu, Y.; Muller, D. A.; DiSalvo, F. J.; Abruña, H. D., Structurally ordered intermetallic platinum–cobalt core–shell nanoparticles with enhanced activity and stability as oxygen reduction electrocatalysts. *Nature Materials* **2013,** *12* (1), 81-87.

4. Kim, H. Y.; Kwon, T.; Ha, Y.; Jun, M.; Baik, H.; Jeong, H. Y.; Kim, H.; Lee, K.; Joo, S. H., Intermetallic PtCu Nanoframes as Efficient Oxygen Reduction Electrocatalysts. *Nano Letters* **2020,** *20* (10), 7413-7421.

5. Gatalo, M.; Bele, M.; Ruiz-Zepeda, F.; Šest, E.; Šala, M.; Kamšek, A. R.; Maselj, N.; Galun, T.; Jovanovič, P.; Hodnik, N., A Double-Passivation Water-Based Galvanic Displacement Method for Reproducible Gram-Scale Production of High-Performance Platinum-Alloy Electrocatalysts. *Angew. Chem. Int. Ed.* **2019,** *131* (38), 13400-13404.

6. Ye, X.; Shao, R.-Y.; Yin, P.; Liang, H.-W.; Chen, Y.-X., Ordered Intermetallic PtCu Catalysts Made from Pt@Cu Core/Shell Structures for Oxygen Reduction Reaction. *Inorganic Chemistry* **2022,** *61* (38), 15239-15246.

7. Zhao, X.; Cheng, H.; Song, L.; Han, L.; Zhang, R.; Kwon, G.; Ma, L.; Ehrlich, S. N.; Frenkel, A. I.; Yang, J.; Sasaki, K.; Xin, H. L., Rhombohedral Ordered Intermetallic Nanocatalyst Boosts the Oxygen Reduction Reaction. *ACS Catalysis* **2021,** *11* (1), 184-192.

8. Wang, C.; Sang, X.; Gamler, J. T.; Chen, D. P.; Unocic, R. R.; Skrabalak, S. E., Facet-dependent deposition of highly strained alloyed shells on intermetallic nanoparticles for enhanced electrocatalysis. *Nano Letters* **2017,** *17* (9), 5526-5532.

9. Gatalo, M.; Ruiz-Zepeda, F.; Hodnik, N.; Drazic, G.; Bele, M.; Gaberscek, M., Insights into thermal annealing of highly-active PtCu3/C Oxygen Reduction Reaction electrocatalyst: An in-situ heating transmission Electron microscopy study. *Nano Energy* **2019,** *63*, 103892.

10. Gong, M. X.; Xiao, D. D.; Deng, Z. P.; Zhang, R.; Xia, W. W.; Zhao, T. H.; Liu, X. P.; Shen, T.; Hu, Y. Z.; Lu, Y.; Zhao, X.; Xin, H. L.; Wang, D. L., Structure evolution of PtCu nanoframes from disordered to ordered for the oxygen reduction reaction. *Appl. Catal., B* **2021,** *282*, 119617.

11. Du, X.; Sun, S.; Ma, G.; Yu, H.; Wang, M.; Lu, Z.; Yu, X.; Li, L.; Zhang, X.; Yang, X., Cu-template-dependent synthesis of PtCu nanotubes for oxygen reduction reactions. *International Journal of Hydrogen Energy* **2022,** *47* (9), 6217-6226.

12. Wang, M.; Zhang, W.; Wang, J.; Minett, A.; Lo, V.; Liu, H.; Chen, J., Mesoporous hollow PtCu nanoparticles for electrocatalytic oxygen reduction reaction. *J. Mater. Chem. A* **2013,** *1* (7), 2391-2394.

13. Oezaslan, M.; Strasser, P., Activity of dealloyed PtCo3 and PtCu3 nanoparticle electrocatalyst for oxygen reduction reaction in polymer electrolyte membrane fuel cell. *Journal of Power Sources* **2011,**

196 (12), 5240-5249.

14. Zhu, G.; Liu, J.; Li, S.; Zuo, Y.; Li, D.; Han, H., Nickel-ion-oriented fabrication of Spiny PtCu alloy octahedral nanoframes with enhanced electrocatalytic performance. *ACS Appl. Energy Mater.* **2019,** *2* (4), 2862-2869.

15. Chen, R.; Shu, T.; Zhao, F.; Li, Y.; Yang, X.; Li, J.; Zhang, D.; Gan, L.-Y.; Yao, K. X.; Yuan, Q., PtCu3 nanoalloy@porous PWOx composites with oxygen container function as efficient ORR electrocatalysts advance the power density of room-temperature hydrogen-air fuel cells. *Nano Res.* **2022,** *15* (10), 9010-9018.

16. Luo, Q.; Xu, W.; Tang, S., Fabricating high-loading ultra-small PtCu3/rGO via a traceless protectant and spray-freeze-drying method. *J. Mater. Chem. A* **2022,** *312*, 121433.

17. Strasser, P.; Koh, S.; Anniyev, T.; Greeley, J.; More, K.; Yu, C. F.; Liu, Z. C.; Kaya, S.; Nordlund, D.; Ogasawara, H.; Toney, M. F.; Nilsson, A., Lattice-strain control of the activity in dealloyed core-shell fuel cell catalysts. *Nat. Chem.* **2010,** *2* (6), 454-460.

18. Xia, B. Y., Boosting Oxygen Reduction via Integrated Construction and Synergistic Catalysis of Porous Platinum Alloy and Defective Graphitic Carbon. *Angewandte Chemie International Edition* **2021,** *20* (8), 25530-25537.

19. Srivastava, R.; Mani, P.; Hahn, N.; Strasser, P., Efficient oxygen reduction fuel cell electrocatalysis on voltammetrically dealloyed Pt–Cu–Co nanoparticles. *Angewandte Chemie International Edition* **2007,** *46* (47), 8988-8991.

20. Qin, Y.; Zhang, W.; Guo, K.; Liu, X.; Liu, J.; Liang, X.; Wang, X.; Gao, D.; Gan, L.; Zhu, Y., Fine-tuning intrinsic strain in penta-twinned Pt–Cu–Mn nanoframes boosts oxygen reduction catalysis. *Advanced Functional Materials* **2020,** *30* (11), 1910107.

21. Tu, W.; Luo, W.; Chen, C.; Chen, K.; Zhu, E.; Zhao, Z.; Wang, Z.; Hu, T.; Zai, H.; Ke, X.; Sui, M.; Chen, P.; Zhang, Q.; Chen, Q.; Li, Y.; Huang, Y., Tungsten as "Adhesive" in Pt2CuW0.25 Ternary Alloy for Highly Durable Oxygen Reduction Electrocatalysis. *Advanced Functional Materials* **2020,** *30* (6), 1908230.